Global MHD simulations of the strongly driven magnetosphere: Modeling of the transpolar potential saturation

V. G. Merkin,[1] A. S. Sharma,[2] K. Papadopoulos,[2] G. Milikh,[2] J. Lyon,[3] and C. Goodrich[1]

Received 23 December 2004; revised 19 May 2005; accepted 1 June 2005; published 1 September 2005.

[1] When the magnetosphere-ionosphere system is driven strongly by the solar wind, the ionospheric transpolar potential tends to saturate. The global MHD simulations are used to study this phenomenon and, in particular, the role the ionospheric conductance plays in controlling the dayside reconnection and the transpolar potentials. The feedback of the ionospheric conductance enhanced due to a high solar wind activity leads to changes in the global configuration of the solar wind-magnetosphere-ionosphere system. The changes in the size of the magnetopause and the associated reconfiguration of the magnetosheath flow lead to a reduction of the reconnection and consequently the transpolar potentials. Thus the solar wind has two competing effects on the transpolar potential, namely, the direct amplification by the solar wind electric field and the feedback of the ionospheric conductance on the reconnection potential.

Citation: Merkin, V. G., A. S. Sharma, K. Papadopoulos, G. Milikh, J. Lyon, and C. Goodrich (2005), Global MHD simulations of the strongly driven magnetosphere: Modeling of the transpolar potential saturation, *J. Geophys. Res.*, *110*, A09203, doi:10.1029/2004JA010993.

1. Introduction

[2] The transpolar potential is by definition the difference between the maximum and the minimum electrostatic potential in the polar ionosphere. Since the magnetospheric convection (among other processes such as neutral winds) drives the ionospheric convection, the transpolar potential (henceforth we will occasionally denote it as Φ_{PC}) is a significant indicator of the solar wind-magnetosphere-ionosphere (SW-M-I) coupling.

[3] It is usually assumed that the transpolar potential varies linearly with the solar wind convective electric field. *Reiff and Luhmann* [1986] noted that for the southward interplanetary magnetic field (IMF), 80–95% of the total cross polar cap voltage variation is due to reconnection at the dayside magnetopause, and the contribution of the viscous processes and tail-lobe merging is typically less than 10 kV. In the ideal MHD model under steady state conditions the electrostatic potential is mapped from the dayside reconnection line to the polar cap. Since the reconnection potential is proportional to the electric field in the magnetosheath, one expects a linear dependence of the transpolar potential on the solar wind electric field under assumption (not obvious, however) of a simple linear relationship between the electric field in the magnetosheath and in the solar wind.

[4] However, a number of observational studies have suggested that Φ_{PC} tends to saturate with increasing electric field in the solar wind [e.g., *Hairston et al.*, 2003; *Russell et al.*, 2000, 2001; *Shepherd et al.*, 2002]. The effect seems counterintuitive and is hard to test experimentally, since the conditions under which it occurs are rather rare.

[5] Many global MHD models predict saturation of the transpolar potential [*Raeder et al.*, 2001; *Siscoe et al.*, 2002b; *Merkin et al.*, 2003], which implies that the effect can, at least partly, be described within the ideal MHD domain. Here, the term "ideal MHD" is used to denote the presumed property of global MHD codes to map the electrostatic potential along magnetic field lines (see section 2). In the strict sense, however, these codes do not solve the system of ideal MHD equations everywhere in the computational domain due to numerical effects, such as those allowing magnetic merging to occur in simulations, and, possibly, parameterized nonideal processes such as the calculation of the ionospheric conductance [e.g., *Fedder et al.*, 1995]. Below, the term "ideal MHD" is used in relation to global MHD simulations in this sense. The ideal MHD description imposes strict limitations on the ways the system evolves. The necessity for the reconnection potential to match the transpolar potential leads to a self-consistent evolution of all the components of the SW-M-I system. A change in the transpolar potential is accompanied by a reconfiguration of the entire system needed to accommodate the new conditions, so that the dayside reconnection potential takes a value consistent with the value of the transpolar potential [*Merkin et al.*, 2003].

[6] This paper presents a comprehensive model of the chain of events accompanying the saturation of the transpolar potential from the solar wind to the ionosphere, based on global MHD simulations. This model is based on: (1) the assumption of the ideal MHD description of the Φ_{PC}

[1]Center for Space Physics, Boston University, Boston, Massachusetts, USA.
[2]Department of Astronomy, University of Maryland, College Park, Maryland, USA.
[3]Department of Physics and Astronomy, Dartmouth College, Hanover, New Hampshire, USA.

0148-0227/05/2004JA010993$09.00

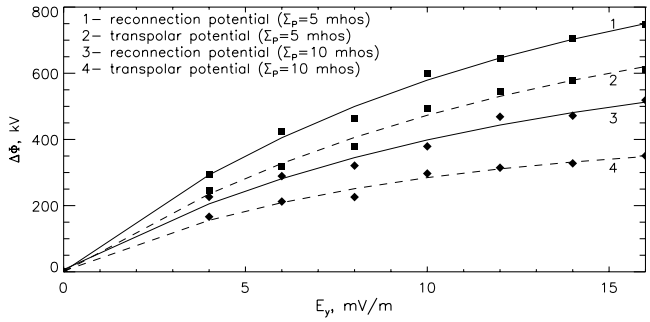

Figure 1. Dependencies of the transpolar and reconnection potentials, $\Delta\Phi$, on the solar wind convective electric field, E_y for the shown values of the ionospheric Pedersen conductance, Σ_P, calculated using the LFM global MHD model. The lines are fits to the simulation data [from *Merkin et al.*, 2003].

saturation and (2) the recognition of the role of the ionospheric conductance in the SW-M-I coupling and, in particular, in the effect of Φ_{PC} saturation. The first assumption suggests the use of global MHD simulations to study the problem at hand. The results discussed here were obtained using the Lyon-Fedder-Mobarry (LFM) global MHD model [*Lyon et al.*, 2004].

[7] The significance of the role of the ionospheric conductance Σ_P in the saturation of the transpolar potential is justified by the following considerations. First, the saturation occurs under conditions of highly disturbed magnetosphere-ionosphere driven by a strong solar wind convective electric field. Under these conditions the ionospheric conductance is generally higher than during quiet periods, due to the energetic particle precipitation or the development of the Farley-Buneman instability at the electrojet altitudes which produces strong anomalous electron heating [*Ossakow et al.*, 1975; *Kelley*, 1989; *Dimant and Milikh*, 2003].

[8] Further, an increase in the ionospheric conductance has an adverse effect on the transpolar potential, which was noted earlier in the simulations using the LFM code [*Fedder and Lyon*, 1987; *Merkin et al.*, 2003; *Merkin et al.*, 2005] as well as other MHD codes [e.g., *Siscoe et al.*, 2002b]. In addition, *Ober et al.* [2003] compared two events having similar solar wind ram pressure and electric field, but different F10.7 flux, which is a proxy of the ionospheric conductance. That study also noted a negative effect of the elevated ionospheric conductance on the transpolar potential.

[9] It should be noted that in the simulations the SW-M-I system behaves neither as a pure voltage generator nor as a current generator and thus Φ_{PC} is neither constant nor is it simply proportional to $1/\Sigma_P$ as Σ_P varies. A reason for such a behavior is that the ionosphere partially controls reconnection on the dayside magnetopause [*Fedder and Lyon*, 1987; *Merkin et al.*, 2003] and thus the system can be described as a voltage generator with a feedback from the load on the generator. This effect of the ionospheric conductance makes it necessary for a model of the transpolar potential saturation to incorporate the feedback of the conductance on the reconnection and transpolar potentials. The paper presents a detailed study of such a feedback and the associated self-consistent processes inferred from the LFM simulations.

[10] This paper makes use of two sets of LFM simulations accomplished by *Merkin et al.* [2003, 2005], as well as a separate set of simulations to study the ram pressure dependence (see section 5). All of these simulations used a steady solar wind input as the inflow boundary condition for the LFM code. The solar wind parameters used are specified in the above references and the corresponding sections of this paper. The ionospheric part of the simulation was carried out with a Pedersen conductance uniform over the entire polar cap and was different for different runs to separate the effect of the ionospheric conductance on the transpolar potential. The Hall conductance was set to zero. In every case, the simulation was run long enough to reach a steady state and the corresponding transpolar potential was averaged over 40 minutes during the steady state. The most recent and exhaustive description of the LFM model can be found in the work of *Lyon et al.* [2004].

2. Dayside Reconnection and Transpolar Potentials

[11] In order to analyze the ionospheric conductance feedback on the reconnection potential it is important to first verify that the MHD model actually maps the potential along the field lines. *Merkin et al.* [2003] used the LFM model to study the dependence of the transpolar and reconnection potentials on the varying convective electric field in the solar wind. Those simulation runs were for the completely symmetric case, i.e., the solar wind flow was strictly antisunward and the IMF was due southward, the solar wind electric field, E_y, was equal to 4, 6, 8, 10, 12, 14, and 16 mV/m, and each simulation was repeated for two values of the ionospheric conductance, viz. 5 and 10 S. The main conclusion was that the simulated transpolar potential tends to saturate, the reconnection potential virtually matches the transpolar potential with the relatively small difference given by the parallel potential drops (due to numerical effects), and the level of saturation depends strongly on the ionospheric conductance (Figure 1).

[12] The technique for the calculation of the simulated reconnection potential involved integration of the parallel electric fields, that are of numerical origin, along the two magnetic field lines connected to the loci of the extrema of the electrostatic potential on the inner boundary of the code. The potential drop between two points lying on the two field lines is given by $\Delta\Phi = \Phi_{PC} + \Phi_{\parallel}^{(1)} + \Phi_{\parallel}^{(2)}$, where $\Phi_{\parallel}^{(1,2)}$ are the parallel potential drops along the field lines. In this representation the two quantities are positive, i.e., the electric field is integrated in opposite direction along the two field lines. For two symmetric points (e.g., the ends of the reconnection line), the potential difference reads $\Delta\Phi = \Phi_{PC} + 2\Phi_{\parallel}$. The dependence of $\Delta\Phi$ on the distance from the inner boundary along the field lines is shown in Figure 2. The curves in the left plot from bottom to top represent simulation runs with the solar wind electric field, E_y = 4, 6, 8, 10, 12, 14, 16 mV/m, respectively, and Σ_P = 5 S. The right plot shows the same for Σ_P = 10 S. Points corresponding to d = 0 lie on the inner boundary and represent the corresponding transpolar potential while the rightmost points (maximum value of d) correspond to the

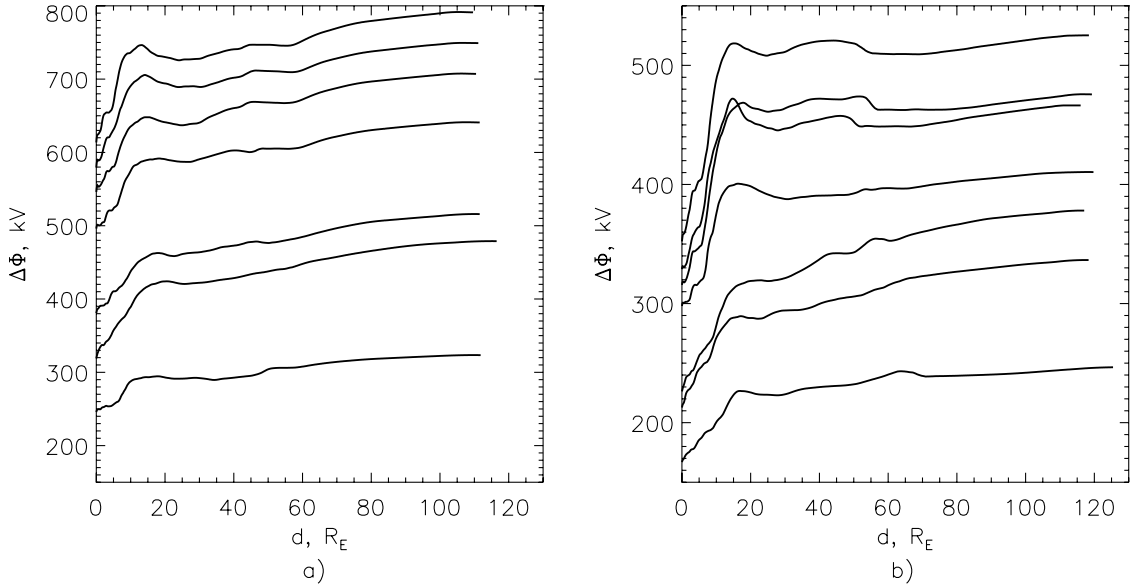

Figure 2. Potential drop between the field lines, $\Delta\Phi$, as a function of the distance from the inner boundary along the field line, d. The leftmost point on every curve lies on the inner boundary and represents the corresponding transpolar potential; the rightmost point corresponds to the potential difference between the field lines in the solar wind. (a) $\Sigma_P = 5$ S. (b) $\Sigma_P = 10$ S. On both plots the curves with the corresponding transpolar potential from bottom to top represent simulation runs with $E_y = 4$, 6, 8, 10, 12, 14, 16 mV/m, respectively.

potential difference between the field lines in the solar wind which we will refer to as the reconnection potential as explained below.

[13] The presence of numerical field-aligned potential drops is responsible for the fact that the reconnection and the transpolar potentials do not coincide completely. The difference between the corresponding solid and dashed lines in Figure 1 is $2\Phi_{||}$ in the above notation. In fact, the solid lines in Figure 1 represent overestimates of the reconnection potential since *Merkin et al.* [2003] continued integration of the parallel electric field until the field lines reached the simulation boundary. The highest parallel potential drop among the simulation runs obtained by such a procedure was estimated to be about 90 kV of which 50–60 kV drop occurred inside the magnetopause. In general, the parallel potential drops are much higher inside the magnetopause than outside of it, which is illustrated by Figure 2 where $\Delta\Phi$ grows faster for d 10–15 R_E (approximate location of the crossing of the field lines with the magnetopause).

[14] An attempt to calculate the reconnection potential more accurately raises new issues. The procedure described above is subject to several sources of errors. First, the footprints of the field lines that connect to the ends of the reconnection line should be chosen carefully. Owing to numerical uncertainties tracing the field lines precisely from the locations of the extrema of the potential on the inner boundary of the code results in the field lines that do not connect exactly to the ends of the reconnection line. Further, once the footprints have been carefully chosen the problem of finding the crossing of the field line with the magnetopause arises. As discussed earlier the computed field-aligned electric fields are naturally higher inside of the magnetopause than outside of it. Thus the integration can be performed up to a point where the parallel electric field significantly reduces. Evidently, the choice of such a point is associated with some ambiguity, as can be seen in Figure 2. Finally, the parallel potentials calculated along the two field lines are not quite symmetric, contrary to what one expects in the completely symmetrical case simulated. Considering all the errors, the uncertainty in the reconnection potential may be up to about 50 kV. Any of these techniques result in a plot similar to Figure 1 with the solid lines lying, as expected, lower than the ones in Figure 1. However, taking into account all the uncertainties in such calculations of the reconnection potential, it is more reasonable to use the upper estimate of the reconnection potential instead, which is the potential difference between the field lines calculated at the edge of the code grid. The uncertainty in the potential difference is less than that in the reconnection potential determined as described above. Figure 1 shows that the upper estimate on the reconnection potential saturates similar to the transpolar potential, and thus this is even more true for the reconnection potential, which is a priori smaller than the potential shown in Figure 1.

3. Effect of the Ionospheric Conductance and Field-Aligned Currents on the Transpolar Potential and the Magnetopause Size

[15] The negative effect of the ionospheric conductance on the transpolar potential is seen in Figure 1. It is important to note that according to Figure 1 the ionospheric conductance provides a feedback not only on the transpolar potential but also on the reconnection potential, as expected in the ideal MHD model (note the difference between the solid lines as well as the dashed lines in Figure 1). *Merkin et al.* [2003] noted that an increase in the ionospheric conductance for a constant solar wind input led to a stronger

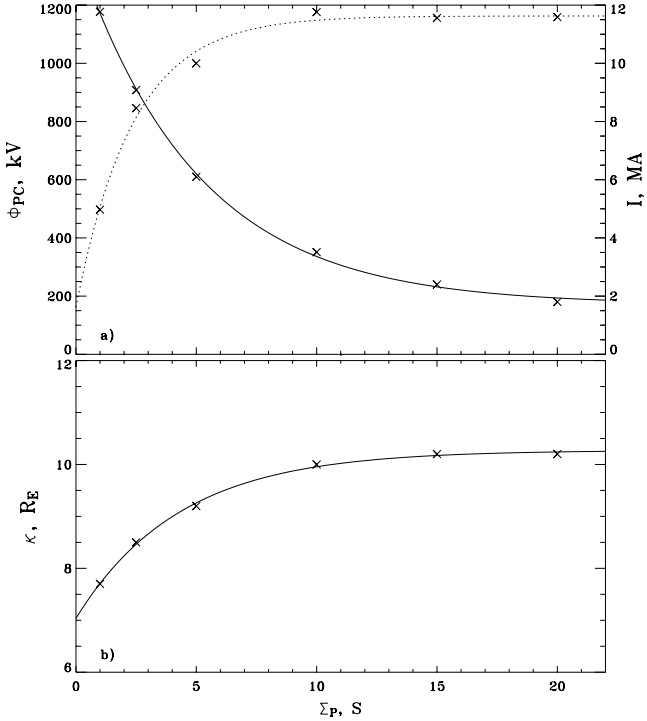

Figure 3. The dependence of (a) the transpolar potential (solid line), the ionospheric integrated field-aligned current (dashed line), and (b) of the magnetopause size in the terminator plane, κ [from *Merkin et al.*, 2005].

magnetopause flaring, i.e., the magnetopause was found further from the earth at the flanks for the higher conductance. It was suggested that such a widening of the magnetopause led to a global reconfiguration of the SW-M-I system, whereby the bow shock moved toward the sun providing more room for the magnetosheath flow to brake. As a result the reconnection potential was reduced. Such a reduction in the reconnection potential caused by the enhanced magnetosheath flow stagnation is discussed in detail in the next section.

[16] *Merkin et al.* [2005] addressed the question of the change in the magnetopause geometry by conducting a series of simulations with the constant solar wind input and the ionospheric conductance varying in a wide range. The results of that study are shown in Figure 3. As seen from the figure the effect of the ionospheric conductance noted by *Merkin et al.* [2003] is robust over a wide range of values of the ionospheric conductance: The widening of the magnetopause at the flanks accompanies the drop in the transpolar and reconnection potentials. This effect was explained by *Merkin et al.* [2005] as arising from the field-aligned currents creating additional magnetic pressure at the flanks of the magnetopause and pushing it outward.

[17] Magnetospheric erosion [*Hill and Rassbach*, 1975; *Maltsev and Lyatsky*, 1975] is another effect of the field-aligned currents that is important in this context. This effect is due to the field-aligned currents driving a downward magnetic field at the subsolar point, i.e., reducing the dipole field and hence internal magnetic pressure, which leads to the reduction in the subsolar distance. Therefore magnetospheric erosion results in further broadening of the magnetosheath, which according to *Merkin et al.* [2003] leads to a reduction in the reconnection potential. In addition, as noticed by *Raeder et al.* [2001], the strongly driven magnetosphere develops "shoulders" (*Siscoe et al.* [2002b] mention that these shoulders are a result of the field aligned currents as well), which make the magnetopause a more blunt obstacle and prevent the flow from reaching the reconnection site. In fact, *Siscoe et al.* [2004] conducted a comparative analysis of existing models of the transpolar potential saturation [*Raeder et al.*, 2001; *Siscoe et al.*, 2002a, 2002b; *Merkin et al.*, 2003] and showed that despite different intrinsic mechanisms leading to saturation of the potential, all of them involve limiting the total strength of the field-aligned current, and therefore they are all strongly interrelated.

[18] Owing to the field-aligned currents providing a physical link between the ionosphere and the magnetopause, an increase in the ionospheric conductance causes a flattening of the magnetopause, with the solar wind conditions held constant. This flattening leads to two competing effects: The length of the reconnection line increases but the reconnection electric field decreases due to the stagnation of the magnetosheath flow [*Merkin et al.*, 2003]. The combined result of these effects is discussed in detail in the following section.

4. Magnetopause Size and the Flow in the Magnetosheath

[19] The ionospheric control of the magnetopause size [*Merkin et al.*, 2003, 2005], summarized above, introduced a concept of the magnetopause as an obstacle in the way of

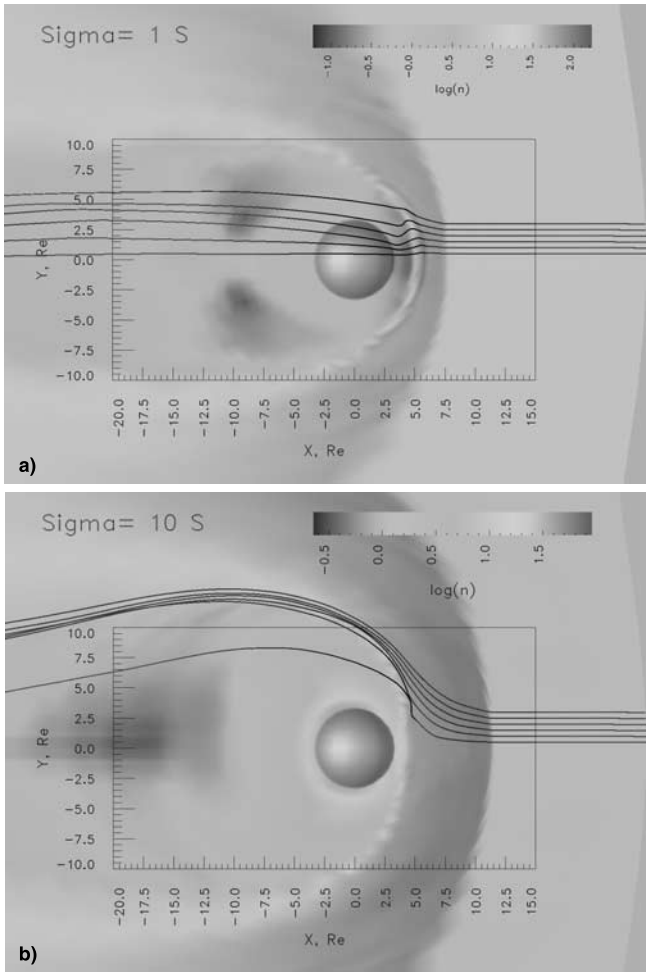

Figure 4. The magnetosphere in the z = 1 plane. The solar wind parameters are $B_z = -40$ nT, $v_x = -400$ km/s, and $n = 30$ cm^{-3}. The background is the plasma mass density on a logarithmic scale. The lines are the projections of 3-D flow streamlines. (a) $\Sigma_P = 1$ S. (b) $\Sigma_P = 10$ S. See color version of this figure at back of this issue.

the solar wind and showed how a change in the size of the obstacle influences the flow in front of it. We now address a question of how the geometry of the magnetopause affects the properties of the magnetosheath flow and the reconnection potential in more detail.

[20] In Figure 4, which illustrates this problem, the magnetosphere is shown in the $z = 1$ plane simulated for $\Sigma_p = 1$ and $\Sigma_p = 10$ S, and the solar wind parameters are $B_z = -40$ nT, $v_x = -400$ km/s, and $n = 30$ cm^{-3}. The background in Figure 4 is the plasma mass density on a logarithmic scale. In addition, streamlines of the flow, originating upstream of the bow shock at points equidistant in the y-coordinate ranging from 0.5 to 3 R_E lying in the plane, are shown. The lines in this figure are, in fact, projections of the three-dimensional streamlines on the plane. Therefore the lines that seem to penetrate the magnetopause actually reach the dayside reconnection line and hence are diverted in the z-direction giving an impression that they get across the magnetopause boundary. Along with the overall differences in the geometry of the system in Figures 4a and 4b, i.e., the size of the magnetopause, the width of the magnetosheath, and the bow shock stand off distance, the figures show how the magnetosheath flow responds to the changes in the geometry of the system. In the case of the greater conductance (the wider magnetopause; see Figure 4b) the deflection of the flow in the magnetosheath is much stronger so that only the streamline originating almost at the symmetry axis reaches the reconnection line while the other streamlines skin the obstacle. Unlike this case, the flow in Figure 4a, corresponding to the smaller ionospheric conductance, experiences almost no deflection in the magnetosheath (in accordance with the small size of the obstacle and thinner magnetosheath) and all the shown streamlines reach the dayside reconnection line.

[21] This picture elucidates why the reconnection potential and consequently the transpolar potential are smaller in the case of the greater ionospheric conductance. In the ideal MHD context, under steady state conditions (constant velocity field), the streamlines are equipotential just like the magnetic field lines. This results from the ideal Ohm's law $\vec{E} = -\frac{1}{c}\vec{v} \times \vec{B}$, which states that the electric field vector is always normal to both the magnetic field and the velocity. A streamline is, by definition, a line tangential to the velocity vector at any point, and therefore, the electric field component parallel to a streamline is identically equal to 0. In an ideal symmetric situation with a southward IMF, as in Figures 4a and 4b, there always exist two ''special'' streamlines that connect to the ends of the dayside reconnection line. The potential difference between these streamlines defines the reconnection potential, and the distance between them upstream of the bow shock is determined by the degree of deflection of the flow in the magnetosheath. We will refer to the segment of the solar wind flow between these lines upstream of the bow shock as the ''image'' of the reconnection line in the solar wind (the linear dimension of this image is the geoeffective distance in the solar wind). The size of this segment is obviously smaller in the situation depicted in Figure 4b than in Figure 4a. This leads to an anti-intuitive conclusion that despite a longer reconnection line in the case of a wider magnetopause, the reconnection potential is actually smaller in this case, since the distance along which the electric field is integrated in the solar wind to obtain the potential drop across the image of the reconnection line is shorter. Note, that the plasma parameters upstream of the bow shock are completely identical in the two cases, and hence, the change in the reconnection potential is determined by the change in the size of the image of the reconnection line.

[22] This approach is basically identical to the explanation of the reconnection potential difference given by *Merkin et al.* [2003]. Changes in the size of the magnetopause, the width of the magnetosheath, and the location of the bow shock are all parts of the same process. A more efficient braking of the magnetosheath flow leading to a drop in the electric field on the nose of the magnetopause is similar to the concept of the stronger deflection of streamlines in the case of a higher ionospheric conductance.

[23] To verify the conclusion about the shrinking of the image of the reconnection line accompanying an increase in the ionospheric conductance we need to extend our study to a larger number of simulated cases. In order to

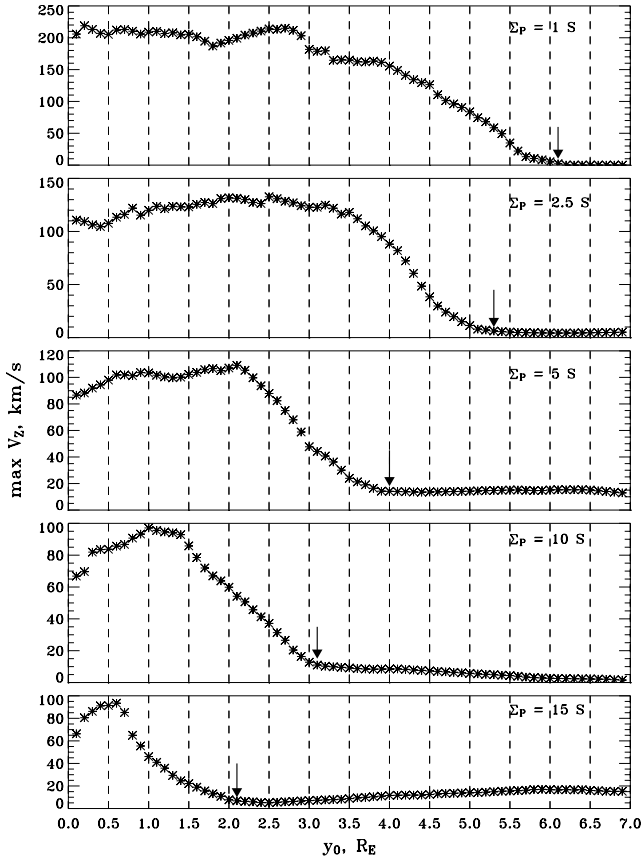

Figure 5. The maximum v_z component of the plasma velocity measured along a streamline originating in the solar wind upstream of the bow shock in the $z = 1$ plane at a distance y_0 from the symmetry axis. The black arrows show the approximate location of the end of the image of the reconnection line (half the geoeffective distance in the solar wind.)

obtain the size of the image of the reconnection line we adopt the following technique. Consider the flow in the equatorial plane. The streamlines originating inside the image are expected to reach the reconnection line, and thus, the z-component of the flow velocity measured along these streamlines should experience a jump as fluid elements moving along the streamlines cross the reconnection region. On the other hand, the streamlines originating outside of the image, are deflected in the same plane and are not expected to have a significant z-component of the velocity. The streamlines that connect to the ends of the reconnection line skin the obstacle. This is unlike a hydrodynamic flow where the boundary of the cross section of the obstacle at the equatorial plane would coincide with the streamline originating infinitely close to the symmetry axis. By measuring the maximum z-component of the velocity along a streamline one can distinguish between the populations of streamlines starting inside and outside of the image of the reconnection line. The results of this procedure are shown in Figure 5. The plots correspond to different values of Σ_P shown in the upper right corner of each plot and the solar wind parameters are the same as in Figure 4. The horizontal axis shows the starting y-positions of streamlines (y_0) while the vertical axis shows the maximum z-component of the plasma velocity measured along a particular streamline. The black arrows indicate an approximate location of the boundary of the image of the reconnection line. The product of the solar wind electric field and $2y_0$ gives the reconnection potential. While it is obvious that no quantitative information can be extracted from these plots due to the broad transition region from high to low maximal v_z, the tendency of the size of the image, as indicated by the black arrows, to shrink with increasing conductance (i.e., the size of the magnetopause) is clear. Note, that v_z does not vanish as y_0 is increased. This is because the shown streamlines originate in the $z = 1$ plane rather than in the equatorial plane.

5. Effect of the Solar Wind Ram Pressure

[24] In order to test the dependence of Φ_{PC} on the solar wind dynamic pressure another set of LFM model runs was conducted. In these runs the solar wind electric field magnitude was kept constant while the density, the magnetic field, and the plasma velocity were varied (see Table 1). The code was run until the system reached a steady state and the magnitude of Φ_{PC} was averaged over about 40 min during the steady state.

[25] Figure 6 shows the results of the simulation. The two top lines represent the best linear fits to the simulation data shown with asterisks, while the two lines at the bottom represent the corresponding dependence given by the Hill/Siscoe model [*Siscoe et al.*, 2002b] for the same set of parameters. The figure indicates a weak dependence of the transpolar potential on the solar wind dynamic pressure in the LFM simulations. In the case of the higher conductance the slope of the line is positive while for the lower conductance it is negative. While this can be a result of numerical errors it is clear that no conclusion can be made about the scaling of Φ_{PC} with dynamic pressure in the LFM simulations from this plot. It should be noted, that, as seen in the figure, the LFM simulation results are in qualitative agreement with the Hill/Siscoe model: In the chosen range of parameters the dependence of the transpolar potential on the solar wind ram pressure in this model is either absent or weak. This behavior can also be seen in the work of *Siscoe et al.* [2002a, Figure 1], which shows that the LFM simulation data seen in Figure 6 are not in the saturation domain defined by the Hill/Siscoe model.

[26] Among the quantitative differences, the overall higher potential produced by the LFM model is worth noticing as well as the ~25% stronger dependence of the transpolar potential on the ionospheric conductance: roughly, $\sim(550-330)/330 = 67\%$ for the LFM and $\sim(280-200)/200 = 40\%$ for Hill/Siscoe. The former discrepancy could be explained by the fact that the coefficients

Table 1. Solar Wind Plasma Parameters Used in the Simulation of the Φ_{PC} Dependence on the Solar Wind Dynamic Pressure

Run Number	1	2	3	4	5
B_z, nT	−25	−20	−15	−25	−30
V_x, km/s	−480	−600	−800	−480	−400
n, cm^{-3}	20	20	20	30	20
E_y, mV/m	12	12	12	12	12

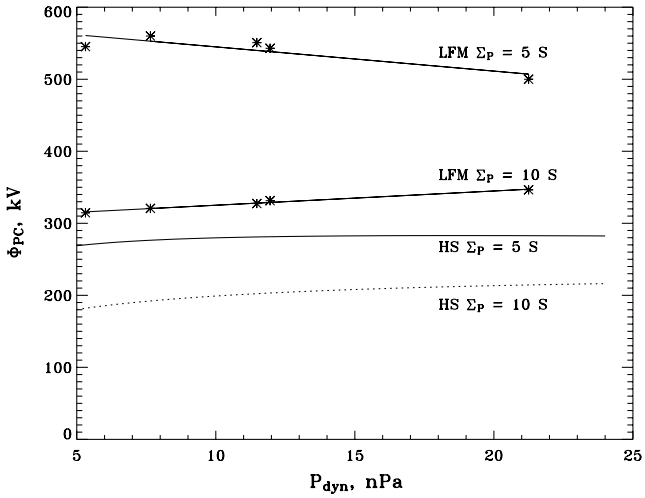

Figure 6. The two top lines show the dependence of the steady state LFM transpolar potential on the solar wind dynamic pressure for the shown values of the ionospheric conductance and E_y = 12 mV/m for the solar wind electric field. The lines represent the best linear fit to the simulation data shown with asterisks. The solar wind parameters for these simulations are summarized in Table 1. The two lines marked "HS" represent the Hill/Siscoe transpolar potential given by *Siscoe et al.* [2002b, equation (13)] for the same set of parameters.

in the Hill/Siscoe model were tuned to the ISM simulation runs driven by a smaller solar wind electric field [*Siscoe et al.*, 2002b] than the LFM simulations presented in this section. On the other hand, *Siscoe et al.* [2002a] showed that even under a more extreme driving (IEF = 15 mV/m), and at approximately the same ionospheric conductance as one of the values chosen for the LFM simulation runs (Σ_P = 12 S) ISM simulation results fit the Hill/Siscoe model quite well. The quantitative discrepancy between the transpolar potentials predicted by the ISM and LFM simulations driven by seemingly similar set of parameters is a separate issue and will not be considered here. However, the relative effect of the ionospheric conductance discussed above is important in the context of this paper and is addressed below.

[27] It is worth noting, that in the presented range of parameters the weak dependence of the LFM transpolar potential on the solar wind ram pressure may be explained by the results discussed in the previous section: While the solar wind dynamic pressure works to compress the magnetopause (Chapman-Ferraro scaling) and shorten the dayside reconnection line, a smaller magnetopause deflects the flow less effectively and the geoeffective distance in the solar wind is larger in this case. Thus, although the reconnection line shrinks as the dynamic pressure increases, its image in the solar wind grows, and the negative effect of the dynamic pressure on the reconnection potential is compensated.

6. Comparison With the Hill/Siscoe Model

[28] This paper discusses the effect of the transpolar potential saturation with emphasis on the role of ionospheric conductance in this process. The Hill/Siscoe model [*Siscoe et al.*, 2002b] provides a framework in which such a model can be analyzed, since it formulates an expression for the unsaturated dayside reconnection potential as given by *Siscoe et al.* [2002b, equation (5)]:

$$\Phi_M \simeq \chi L_r E_{sw} p_{sw}^{-1/6} D^{1/3} F(\theta), \tag{1}$$

where the coefficient χ describes magnetosheath compression and reconnection efficiency, and the other terms are discussed by *Siscoe et al.* [2002b]. The Hill/Siscoe model postulates that the saturated transpolar potential is smaller than Φ_M, which means that the saturated dayside reconnection potential is no longer given by formula (1), and the physics behind this equation (specifically, behind the coefficient χ) breaks down as the system approaches the state of saturation. The Hill/Siscoe model describes a mechanism of saturation but does not discuss specifically which of the processes included in equation (1) fails under strong solar wind driving. The model discussed in this paper suggests a physical process not covered by equation (1), namely, the effect of the ionospheric conductance on the size of the magnetopause at the flanks and the consequent reconfiguration of the magnetosheath flow affecting the geoeffective potential in the solar wind. As noted by *Merkin et al.* [2005], magnetospheric erosion [*Hill and Rassbach*, 1975; *Maltsev and Lyatsky*, 1975] complements the ionospheric conductance effect discussed in this paper in reducing the dayside reconnection potential, and thus it is another mechanism contributing to breaking down the physics of equation (1).

[29] These processes can compensate the lack of dependence of the Hill/Siscoe saturated transpolar potential on the conductance (as compared to the LFM potential), indicated in section 5. To verify this conjecture we test the Hill/Siscoe model against the LFM simulations conducted by *Merkin et al.* [2003] shown in Figure 1. In order to proceed with the comparison we rewrite an equation from *Siscoe et al.* [2002b, equation (13)] in the following form:

$$\Phi_{PC}(\mathrm{kV}) = \frac{\alpha E_{sw} p_{sw}^{1/3} D^{4/3} F(\theta)}{p_{sw}^{1/2} D + \beta \xi \Sigma_P E_{sw} F(\theta)} + \Phi_0, \tag{2}$$

where the coefficients α and β given by [*Siscoe et al.*, 2002b] are 57.6 and 0.01, respectively. In addition, we have added a constant term Φ_0 which is common for empirical forms of the transpolar potential dependence on the solar wind driving function [*Reiff and Luhmann*, 1986; *Boyle et al.*, 1997; *Burke et al.*, 1999]. The coefficients α = 57.6 and β = 0.01 are derived based on physical considerations and cannot be changed freely in the theory by *Siscoe et al.* [2002b]. However, by allowing them to vary we search for values of α, β, and Φ_0 providing the best least squares fit to the LFM simulation data.

[30] It turns out that the least square error function has multiple local minima so that it is impossible to derive a unique set of values of $\{\alpha, \beta, \Phi_0\}$ that provide the best fit of the function in equation (2) to the simulation data. This problem is overcome by using the following procedure. We find the range of parameters resulting in error function lower than some threshold, e.g., 20% of the minimum

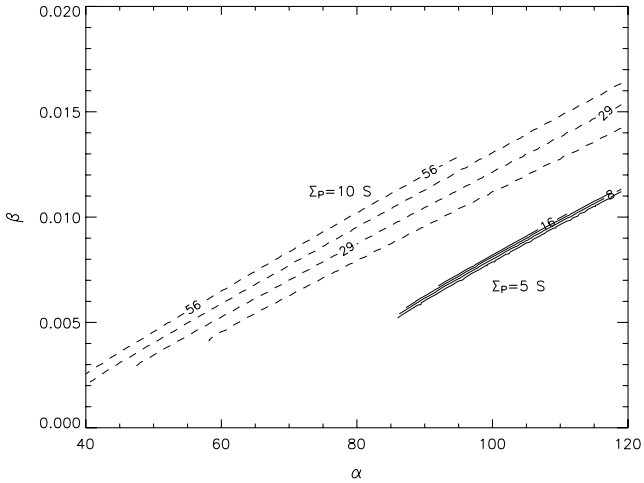

Figure 7. Contours of the constant term Φ_0 in α, β space. The parameters shown here result in the least squares error function, which is less or equal than 20% of the minimum transpolar potential simulated for a given value of the ionospheric conductance. The dashed lines represent Σ_P = 10 S, while the solid lines are for Σ_P = 5 S. The contours are labeled according to Φ_0.

transpolar potential simulated for a given value of the ionospheric conductance (shown in Figure 1), and plot Φ_0 as a function of α and β in this range for the two values of the ionospheric conductance used in the simulations. The results of this procedure are shown in Figure 7. The solid contours show values of Φ_0 for Σ_P = 5 S while the dashed contours show the same for Σ_P = 10 S. The parameter range shown obviously contains unphysical solutions, for example, those with too high values of Φ_0. However, the fact that the two regions marked by the solid and dashed contours do not overlap means that there is no unique triple $\{\alpha, \beta, \Phi_0\}$ that would fit the LFM simulation data for the two values of the ionospheric conductance. For a fixed value of Φ_0, either α or β should change by a factor of 1.5–2 to obtain a fit of the same quality when the conductance is changed from 5 to 10 S. This result does not necessarily imply that α or β in the Hill/Siscoe model should explicitly depend on the ionospheric conductance. However, it suggests that in order to fit to the LFM simulation data by *Merkin et al.* [2003] the Hill/Siscoe model should have a stronger dependence on the ionospheric conductance, which can, perhaps, be mimicked by including additional parameterized conductance-dependent terms in the denominator of equation (2).

[31] The model of ionospheric conductance feedback on the transpolar potential discussed here provides this additional dependence. In fact, the two models are not mutually exclusive but rather complement each other. Both models are based on the feedback due to the ionospheric conductance to the dayside reconnection potential, although the physical mechanisms of these feedbacks are different. However, the methodological distinction between the models is that the Hill/Siscoe model postulates the expression for the saturated transpolar potential which depends indirectly on the ionospheric conductance through the field-aligned currents. On the other hand, the model described here emphasizes the influence of the increased solar wind activity on the ionospheric conductance which then provides the feedback on the reconnection potential, as discussed in the next section.

[32] *Merkin et al.* [2003] stated that another distinction between the models is in the way they treat the mapping of the electrostatic potential along magnetic field lines. A clarification of this may be in order here. Though not stated clearly in the work of *Siscoe et al.* [2002b], the Hill/Siscoe model implies (G. Siscoe, personal communication, 2005) that the dayside reconnection and the transpolar potentials are the same in both the saturated and unsaturated domains. The statement to the contrary was made by *Merkin et al.* [2003], although the conclusions of that paper, as well as those of the current paper, are not affected by this misinterpretation.

7. A Comprehensive Model of Transpolar Potential Saturation

[33] The global MHD LFM simulations [*Merkin et al.*, 2003, 2005] and the results presented in this paper show a strong interrelationship among the processes in the region from the bow shock to the ionosphere, and suggest a comprehensive model of the saturation of the transpolar potential, as summarized in a diagram shown in Figure 8. The diagram demonstrates, under highly disturbed conditions, the chain of events from the solar wind to the ionosphere, as well as the ionospheric feedback on the global properties of other magnetospheric regions such as the magnetopause, the bow shock, and the magnetosheath. This MHD model provides some insights into the behavior of the SW-M-I system leading to the transpolar potential saturation.

[34] The solar wind influences the transpolar potential via two channels: (1) the solar wind convective electric field (IEF) affects directly the reconnection potential which is mapped to the ionosphere and an increase in the IEF tends to amplify the transpolar potential; (2) on the other hand, the solar wind activity affects the ionospheric conductance either directly through energetic particle precipitation or indirectly through development of the Farley-Buneman or other ionospheric plasma instabilities [*Ossakow et al.*, 1975; *Kelley*, 1989; *Dimant and Milikh*, 2003; *Merkin et al.*, 2004]. An increase in the ionospheric conductance provides a negative feedback on the reconnection potential through the chain of events discussed in the work of *Merkin et al.* [2003, 2005] and in this paper. The components of this chain are summarized in the dashed box on the left panel of Figure 8. An increase of the ionospheric conductance induced by the elevated solar wind activity leads to the growth of the ionospheric field-aligned currents which modify the pressure balance conditions at the flanks of the magnetopause [*Siscoe et al.*, 2002a; *Merkin et al.*, 2005]. The additional magnetic pressure driven by these currents pushes the magnetopause outward creating new boundary conditions for the magnetosheath flow. Further, once the size of the magnetopause increases, the magnetosheath flow reconfigures, the stagnation region broadens, and the reconnection potential is reduced (see section 4). Finally, the mapping of the electrostatic potential leads to a reduction of the transpolar potential. The direct effect of the solar wind electric field that increases the reconnection potential is thus

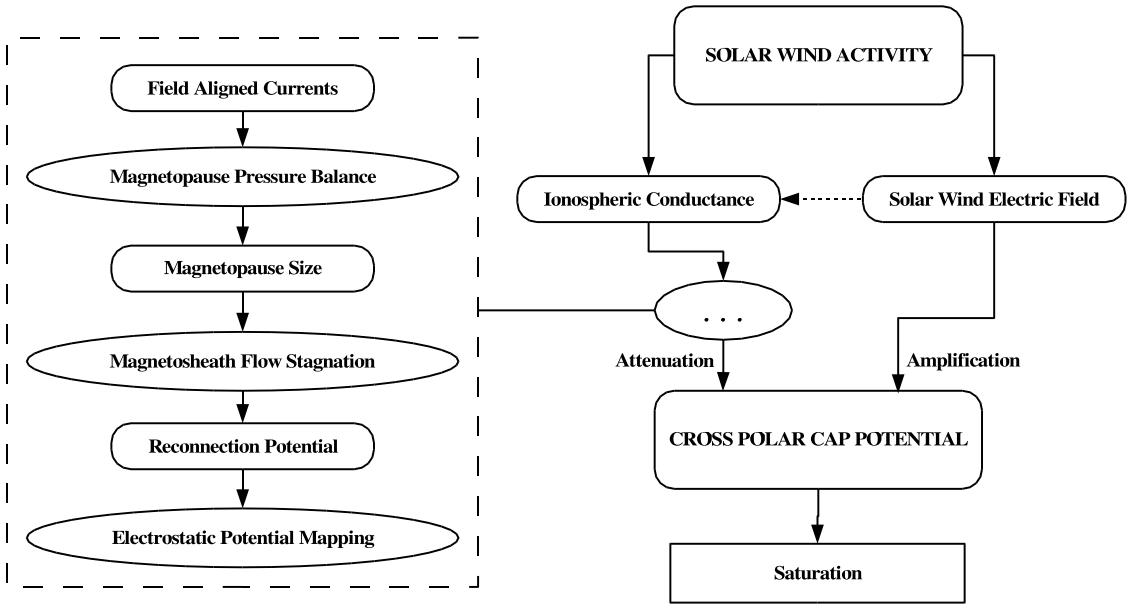

Figure 8. The interrelationship between the different regions and physical processes in the SW-M-I system leading to a comprehensive model of the transpolar potential saturation.

opposed by the feedback effect of the ionospheric conductance, and therefore leads to saturation.

8. Summary

[35] The transpolar potential saturates with an increase in the interplanetary electric field, as shown by observations and models. The feedback of the field-aligned currents to the magnetic reconnection at the magnetopause was first recognized by *Hill et al.* [1976] as the mechanism for the saturation. *Siscoe et al.* [2002b] elaborated on that model and expressed the Hill potential in terms of the variables describing the reconnection and related current systems, and compared the results to global MHD simulations. A study of the role of the ionospheric conductivity in the saturation process, accomplished using the LFM global MHD model, showed the feedback effect due to changes in the ionospheric conductivity [*Merkin et al.*, 2003, 2005].

[36] The MHD simulations, discussed in this paper, show the self-consistent changes in the solar wind-magnetosphere-ionosphere system during the saturation of the transpolar potential. The change in the ionospheric conductance leads to a change in the magnetopause shape and consequently to the reconfiguration of the magnetosheath flow. The self-consistent reduction in the dayside reconnection potential then leads to the transpolar potential saturation.

[37] **Acknowledgments.** This research was supported by NASA grants NAG513452 and NAG510882, and NSF grants ATM0119196 and ATM0334256. We thank NCSA for computational resources used to complete the simulations.

[38] Arthur Richmond thanks Joachim Raeder and another reviewer for their assistance in evaluating this paper.

References

Boyle, C. B., P. H. Reiff, and M. R. Hairston (1997), Empirical polar cap potentials, *J. Geophys. Res.*, *102*, 111–125.

Burke, W. J., D. R. Weimer, and N. C. Maynard (1999), Geoeffective interplanetary scale sizes derived from regression analysis of polar cap potential, *J. Geophys. Res.*, *104*, 9989–9994.

Dimant, Y. S., and G. M. Milikh (2003), Model of anomalous electron heating in the E region: 1. Basic theory, *J. Geophys. Res.*, *108*(A9), 1350, doi:10.1029/2002JA009524.

Fedder, J. A., and J. G. Lyon (1987), The solar wind-magnetosphere-ionosphere current-voltage relationship, *Geophys. Res. Lett.*, *14*, 880–883.

Fedder, J. A., S. P. Slinker, J. G. Lyon, and R. D. Elphinstone (1995), Global numerical simulation of the growth phase and the expansion onset for substorm observed by Viking, *J. Geophys. Res.*, *100*, 19,083–19,093.

Hairston, M. R., T. W. Hill, and R. A. Heelis (2003), Observed saturation of the ionospheric polar cap potential during the 31 March 2001 storm, *Geophys. Res. Lett.*, *30*(6), 1325, doi:10.1029/2002GL015894.

Hill, T. W., and M. E. Rassbach (1975), Interplanetary magnetic field direction and the configuration of the day side magnetopause, *J. Geophys. Res.*, *80*, 1–6.

Hill, T. W., A. J. Dessler, and R. A. Wolf (1976), The role of ionospheric conductivity in the acceleration of magnetospheric particles, *Geophys. Res. Lett.*, *3*, 429–432.

Kelley, M. C. (1989), *The Earth's Ionosphere: Plasma Physics and Electrodynamics*, Elsevier, N. Y.

Lyon, J. G., J. A. Fedder, and C. M. Mobarry (2004), The Lyon-Fedder-Mobarry (LFM) global MHD magnetospheric simulation code, *J. Atmos. Sol. Terr. Phys.*, *66*, 1333–1350, doi:10.1016/j.jastp.2004.03.020.

Maltsev, Y. P., and W. B. Lyatsky (1975), Field-aligned currents and erosion of the dayside magnetopause, *Planet. Space Sci.*, *23*, 1257–1260.

Merkin, V. G., K. Papadopoulos, G. Milikh, A. S. Sharma, X. Shao, J. Lyon, and C. Goodrich (2003), Effects of the solar wind electric field and ionospheric conductance on the cross polar cap potential: Results of global MHD modeling, *Geophys. Res. Lett.*, *30*(23), 2180, doi:10.1029/2003GL017903.

Merkin, V. G., G. Milikh, A. S. Sharma, K. Papadopoulos, J. Lyon, and C. Goodrich (2004), Effect of the anomalous electron heating on the ionospheric potential in the global MHD model, *Eos Trans. AGU*, *85*(47), Fall Meet. Suppl., Abstract SM43A-1142.

Merkin, V. G., A. S. Sharma, K. Papadopoulos, G. Milikh, J. Lyon, and C. Goodrich (2005), Relationship between the ionospheric conductance, field aligned current, and magnetopause geometry: Global MHD simulations, *Planet. Space Sci.*, *53*(9), 873–879, doi:10.1016/j.pss.2005.04.001.

Ober, D. M., N. C. Maynard, and W. J. Burke (2003), Testing the Hill model of transpolar potential saturation, *J. Geophys. Res.*, *108*(A12), 1467, doi:10.1029/2003JA010154.

Ossakow, S. L., K. Papadopoulos, J. Orens, and T. Coffey (1975), Parallel propagation effects on the type 1 electrojet instability, *J. Geophys. Res.*, *80*, 141–148.

Raeder, J., Y. Wang, T. Fuller-Rowell, and H. J. Singer (2001), Global simulation of space weather effects of the Bastille Day storm, *Sol. Phys.*, *204*, 325.

Reiff, P. H., and J. G. Luhmann (1986), Solar wind control of the polar-cap potential, in *Solar Wind-Magnetosphere Coupling*, edited by Y. Kamide and J. A. Slavin, p. 453, Terra Sci., Tokyo.

Russell, C. T., G. Lu, and L. G. Luhmann (2000), Lessons from the ring current injection during the September 24, 25, 1998 storm, *Geophys. Res. Lett.*, *27*, 1371–1374.

Russell, C. T., J. G. Luhmann, and G. Lu (2001), Nonlinear response of the polar ionosphere to large values of the interplanetary electric field, *J. Geophys. Res.*, *106*, 18,495–18,504.

Shepherd, S. G., R. A. Greenwald, and J. M. Ruohoniemi (2002), Cross polar cap potentials measured with Super Dual Auroral Radar Network during quasi-steady solar wind and interplanetary magnetic field conditions, *J. Geophys. Res.*, *107*(A7), 1094, doi:10.1029/2001JA000152.

Siscoe, G. L., N. U. Crooker, and K. D. Siebert (2002a), Transpolar potential saturation: Roles of region 1 current system and solar wind ram pressure, *J. Geophys. Res.*, *107*(A10), 1321, doi:10.1029/2001JA009176.

Siscoe, G. L., G. M. Erickson, B. U. Ö. Sonnerup, N. C. Maynard, J. A. Schoendorf, K. D. Siebert, D. R. Weimer, W. W. White, and G. R. Wilson (2002b), Hill model of transpolar potential saturation: Comparisons with MHD simulations, *J. Geophys. Res.*, *107*(A6), 1075, doi:10.1029/2001JA000109.

Siscoe, G., J. Raeder, and A. J. Ridley (2004), Transpolar potential saturation models compared, *J. Geophys. Res.*, *109*, A09203, doi:10.1029/2003JA010318.

C. Goodrich and V. G. Merkin, Center for Space Physics, Boston University, 725 Commonwealth Avenue, Boston, MA 02215, USA. (vgm@bu.edu)

J. Lyon, Department of Physics and Astronomy, Dartmouth College, 303 Wilder Laboratory, Hanover, NH 03755-3528, USA.

G. Milikh, K. Papadopoulos, and A. S. Sharma, Space and Plasma Physics Group, Department of Astronomy, University of Maryland, College Park, MD 20742-2421, USA.

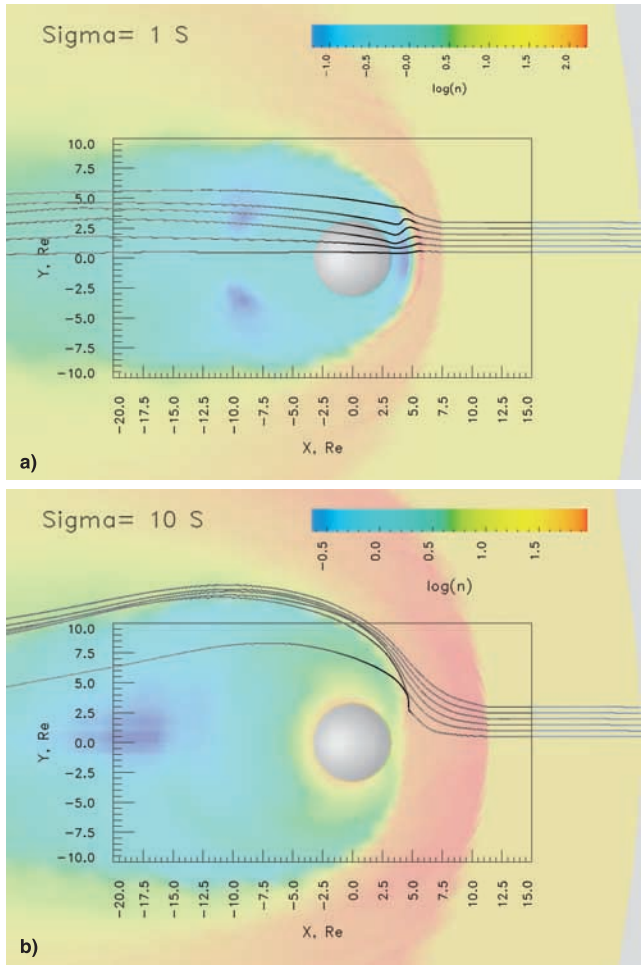

Figure 4. The magnetosphere in the z = 1 plane. The solar wind parameters are $B_z = -40$ nT, $v_x = -400$ km/s, and $n = 30$ cm^{-3}. The background is the plasma mass density on a logarithmic scale. The lines are the projections of 3-D flow streamlines. (a) $\Sigma_P = 1$ S. (b) $\Sigma_P = 10$ S.